Available online at www.sciencedirect.com
SCIENCE DIRECT
International Journal of Mass Spectrometry 254 (2006) 20–27
International Journal of Mass Spectrometry
www.elsevier.com/locate/ijms

Correlated phase space distributions of ions in an orthogonal time-of-flight mass spectrometer

D. Papanastasiou [a,*], A.W. McMahon [b]

[a] *Manchester Metropolitan University, Department of Chemistry and Materials, Manchester, UK*
[b] *University of Manchester, Molecular Imaging Centre, Manchester, UK*

Received 24 March 2006; received in revised form 24 April 2006; accepted 24 April 2006
Available online 5 June 2006

Abstract

A prototype orthogonal time-of-flight (oTOF) mass spectrometer equipped with a thermal ionization (TI) source and an electron impact (EI) source was designed and constructed. Low energy ion beams (∼10 eV) were generated and ejected by a two-stage acceleration configuration into the TOF mass analyzer operating in the linear mode. Interfaces between the sources and the analyzer were optimized so as to reduce the contribution of the turn-around time on the final resolving power of the instrument. The concept of space-velocity correlated ion beams is described in this context. Experiments with variable detector positions were performed and spectral line widths of ∼2 ns were achieved at the end of a 45 cm long linear oTOF MS with ∼3.7 keV energy ions. A new theoretical approach is developed for linear phase space distributions of ions at the start of the TOF experiment. Analytical solutions for first and second-order focusing instruments are presented.

Keywords: Orthogonal time-of-flight mass spectrometry; Space-velocity correlation focusing

1. Introduction

The concept of accelerating ions orthogonal to the direction of propagation of an ion beam [1] has extended the utility of time-of-flight mass spectrometry (TOF MS) to continuous ionization techniques. The ability to monitor continuous processes by TOF MS and to record spectra with uniform mass resolution over a wide mass range are the two main characteristics of an orthogonal time-of-flight (oTOF) mass analyzer. Reduction of the initial volume of the ions prior to mass analysis is considered an essential advantage of this particular configuration. The spatial and velocity distributions in the TOF direction are minimized, offering ideal conditions for high resolving power experiments. Since its re-introduction [2,3], oTOF MS has been established as a mainstream technique in modern mass spectrometry [4–6].

In TOF MS, the arrival time spread of the ions at the detector is limited by two types of energy distributions; the distribution of an ion cloud in terms of the ion's initial potential energies, known as the spatial spread, and that determined by the kinetic energy spread. Space focusing theory [7] is a method to correct for the differences in the drifting velocities and provide isochronous flight times in cases were the initial spatial spread dominates over the starting velocities of the ions. Kinetic energy distributions are more complicated and specific to the instrument configuration. The turn-around time is a mass dependent expression for the maximum contribution of the initial ion velocity to the final arrival time spread [7]. The relative contributions of spatial and kinetic energy spreads to the resolving power of a TOF system are usually considered independently. A special case is that of the delayed extraction technique were a correlation between starting positions and initial ion velocities has been established [8,9].

The orthogonal gate is a two-stage acceleration region, based on the original Wiley and McLaren configuration [7]. The kinetic energy spread of the ions in the direction orthogonal to the beam is in the low meV range and space focusing theory has been used to estimate and apply an optimum set of voltages to a pre-determined geometry [10–13]. Uncorrelated distributions of ions have been considered [14–16] in which case the overall resolving power is determined by the relative contributions of the spatial spread and the turn-around time. A linear correlation between starting positions and ion velocities in the effective

* Corresponding author.
E-mail address: dpapanastasiou@gmail.com (D. Papanastasiou).

1387-3806/$ – see front matter © 2006 Elsevier B.V. All rights reserved.
doi:10.1016/j.ijms.2006.04.014

region of the orthogonal gate has been proposed [17]. An attempt is made herein to provide a concise experimental and theoretical analysis of space-velocity correlation focusing, specific to the oTOF mass analyzer.

Linear instruments have been designed with long field-free regions to enhance resolving power by extending the flight path. The ability to resolve adjacent masses is then limited by the wide arrival time spread of the ions. In reflectron configurations the focal point (virtual source) is projected to shorter distances and resolving power is improved by extending the flight path and simultaneously reducing the time spread of the ions at the detector. Reflectrons are optimized by approximating the virtual source with a focal plane where ions have a distribution in kinetic energies. In a real situation the virtual source has a finite size, determined by the initial spatial and velocity spreads. The ability of an acceleration system to produce high quality virtual sources is essential to fully exploit the focusing properties of reflectrons. Short linear TOF instruments have not been built to investigate such virtual sources and establish whether the reduction in the time spread of the ions is a property of the reflectron or introduced by the two-stage acceleration system.

Coupling two ion sources on the same oTOF mass spectrometer has provided insights on the time-focusing properties of our linear system [18]. The energy distribution of ions generated on the plane of a hot metal surface differs from those formed via electron impact over a finite volume in the source. Variations in the optimum voltages required to minimize the arrival time spread of the ions have been observed and interpreted in terms of the differences in the initial conditions of the ions prior to TOF analysis. We have varied the position of the detector and focusing parameters are examined at the shorter distances that could be used as virtual sources for a reflectron. Narrow spectral line widths are achieved and attributed to space-velocity correlated beams. The ideal situation of a linear dependence between position and velocity of the ions prior to TOF measurement is treated analytically and first and second-order focusing conditions are derived for two-stage linear geometries.

2. Experimental

A schematic diagram of the instrument is shown in Fig. 1(a). A triple filament TI source and an EI source were mounted symmetrically around the orthogonal gate of the oTOF mass analyzer. Ions were sampled independently from each source by rotating the orthogonal gate. The length of field-free region was varied by vertical displacements of the detector. The pressure in the flight tube was $\sim 10^{-9}$ mbar, measured by an ionization gauge.

Samples for the TI source were loaded on the first six-way cross-chamber, designed for filament pre-heating. A magnetic arm carrying the filament holder was used for transferring the filament into the source assembly. TI filaments (Cathodeon, Cambridge, UK) were resistively heated at currents between 2.0 and 5.0 A using a lab-made filament power supply. Accelerating potentials in the range of 5–100 V were applied on a set of lenses and delivered ions through a 1.5 mm slit to the orthogonal acceleration region. The EI source was mounted on a cluster flange, opposite the TI source. A repeller electrode inside the source box and a weak external field facilitated ion extraction. Ions were focused and directed through a 0.7 mm exit slit by two half plates. A thoriated tungsten filament was used to provide the ionizing beam. Ion beam centres were aligned by the two source exit slits, positioned at an equal distance from the effective region of the orthogonal gate. A comparison of the time-focusing properties in the oTOF analyzer between the ion sources was then feasible as both beam energies were ~10 eV.

The two-stage acceleration configuration was defined by four parallel electrodes, as shown in Fig. 1(b). Grids with 1

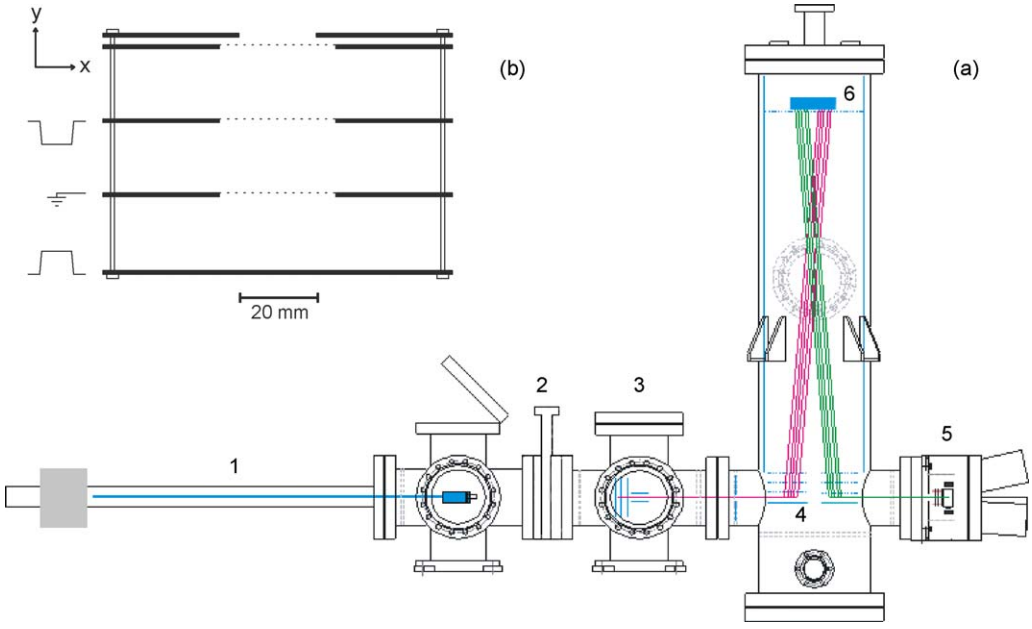

Fig. 1. Instrument schematic diagram (a) showing: 1, magnetic arm; 2, gate valve; 3, thermal ionization source; 4, orthogonal gate; 5, electron impact source; 6, detector and magnified orthogonal gate (b).

wire/350 μm were used to separate adjacent electric fields and the field-free region (Buckbee-Meers, St. Paul, MN, US). In a two-stage oTOF mass spectrometer with a fixed detector position, the turn-around time contribution can be reduced by choosing the second field longer than the first while satisfying space focusing theory. In this case, the total length of the first pulsed field was 38 mm and that of the second 18 mm. The first grid was kept at zero potential (ground) and the back plate with the second grid were pulsed symmetrically by a PVM-4210 high voltage pulse generator (DEI, Fort Collins, CO, US) with a rise time of <12 ns. Ion beams were sampled at a frequency of ∼50 kHz (20 μs pulse period). The second accelerating field was defined by a third grid electrically connected with the flight tube, floated at −3.1 kV. The microchannel plate was a chevron Photek model VPM340. The output signal was amplified with the AC coupled 9306 Ortec 1 GHz preamplifier with typical output rise times of ∼350 ps and digitized by the 9353 Ortec Time-to-Digital Converter with a 100 ps resolution.

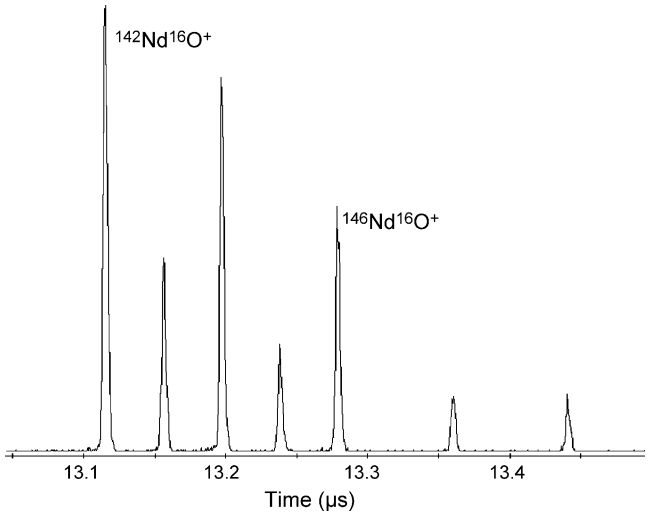

Fig. 3. NdO spectrum each peak with a time spread (FWHM) of 3.15 ns, $R = 2000$.

3. Results and discussion

The time-focusing curves for each source and variable detector distances are presented in Fig. 2 where the arrival time distribution of the ions is plotted as a function of the voltage ratio $\xi = V_s/V_d$, where V_s and V_d are the potentials applied across the first and second fields of length s and d, respectively. The total energy of the ions was maintained at ∼3.5 kV by fixing the flight tube and detector voltage. The time-focusing curves were obtained by scanning the magnitude of the symmetrical extraction pulses applied across the first field. The time dispersion of the ions at the detector exhibit a minimum, specific to the m/z ratio and characteristic of the initial conditions at the onset of the extraction pulse.

Data obtained with the TI source for a 67 cm long field-free region, show a mass independent optimum voltage ratio ($\xi = 0.30$) with a resolving power of >1500 across the atomic mass spectrum. Ions were generated by resistively heating a Re filament loaded with Nd. Flight times for the Nd isotopes are ∼12.4 μs with a spread of the order of ∼4.2 ns (FWHM). Filament impurities were also observed and include Na, K and Sr. The lightest m/z detected is the ^{23}Na ion with a flight time ∼5.1 μs and a time spread of ∼1.6 ns. The NdO spectral lines, generated by running the filament at the lower temperatures, are shown in Fig. 3 and each have a time spread of 3.2 ns (FWHM) demonstrating a resolving power of >2000.

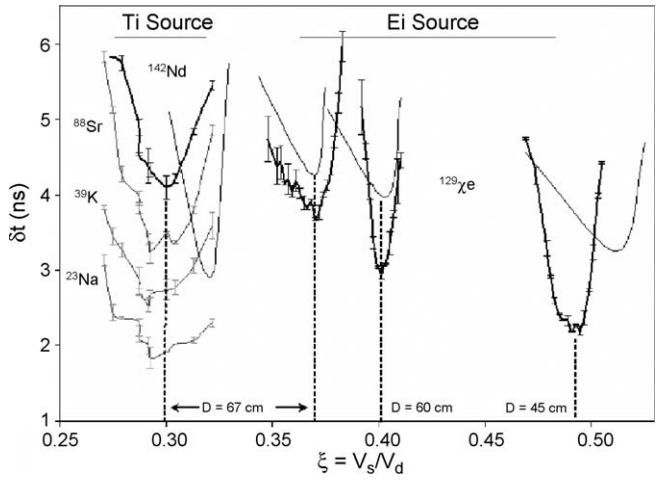

Fig. 2. Experimental time-focusing curves for the TI source at 67 cm and for the EI source at 67, 60 and 45 cm long field-free regions. Time spread is measured at FWHM of the spectral lines. Bars show the maximum error between successive measurements. The solid curves were obtained by one-dimensional TOF calculations.

For the same detector distance and ion beam energy, the optimum voltage ratio for time-focusing the xenon isotopes ionized via electron impact is displaced to higher values ($\xi = 0.37$). The difference in the magnitude of the extraction pulses between the two sources is 150 V for ∼900 V across the first field. Data are shown for the xenon isotope ^{129}Xe. Resolution achieved with the two sources on the 67 cm long configuration is comparable. Despite the fact that ion beams energies are equal, the difference in the magnitude of the optimum voltage ratio indicates that the starting conditions vary and are specific to the source and ion optics employed to deliver ions into the orthogonal gate.

As the detector is displaced to shorter distances the time dispersion for the xenon isotopes is reduced and time-focusing is satisfied by the higher extraction pulses. The shorter the field-free region, the narrower the arrival time spread of the ions at the detector. Fig. 4 shows spectral lines for ^{129}Xe and ^{132}Xe at each of the three distances examined. The voltage ratio increases from 0.37 to 0.40 and finally to 0.49 for the 67, 60 and 45 cm long configurations, respectively. The change in the magnitude of the extraction pulse is from 965 V at 67 cm to 1230 V at 45 cm. An important observation is that the change in the arrival time spread over-compensates for the reduction in the flight time of the ions with an overall enhancement in resolving power R. This is in contrast with the general practice of extending the flight path hence the flight times to improve R. For the 67 cm long configuration the time spread is ∼3.5 ns with $R = 1700$ and reduces by 1.6 ns for the 45 cm configuration with $R = 2200$. Reduction in the time spread of the ions is observed even for the smallest

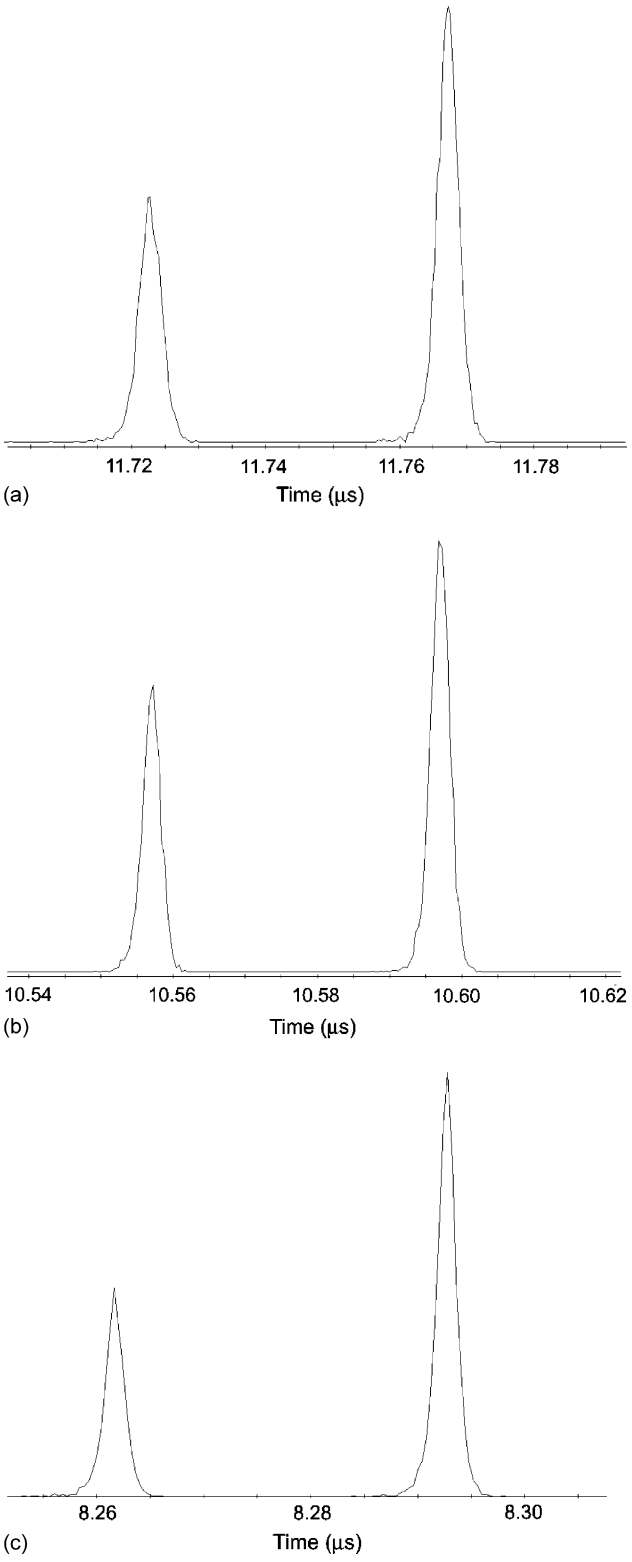

Fig. 4. ^{129}Xe and ^{132}Xe spectral lines at the optimum voltage ratios for each of the three detector distances: (a) $D = 67$ cm, $\delta t = 3.5$ ns (FWHM), $R = 1700$; (b) $D = 60$ cm, $\delta t = 2.9$ ns (FWHM), $R = 1850$; (c) $D = 45$ cm, $\delta t = 1.9$ ns (FWHM), $R = 2200$.

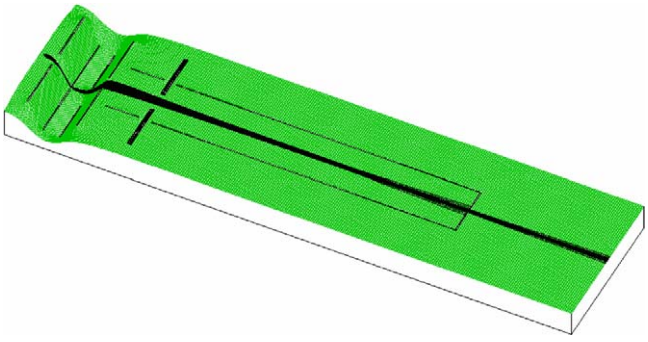

Fig. 5. Potential energy surface of the TI source. The distance from the source to the orthogonal gate is 20 cm.

detector displacement from 67 to 60 cm. TOF mass spectrometers incorporating a reflectron project the virtual source close to the acceleration region. The ability of reflectron oTOF mass spectrometers to produce narrower spectral lines widths can therefore be considered as a property of the two-stage acceleration system.

The spatial and energy distributions of the ions entering the orthogonal gate were modelled using SIMION [19]. Weak accelerating fields directed ions through the lenses so as to create a focal point near the exit slit of the source. The angular divergence of the beam was optimized to minimize the velocity components in the TOF direction while countering turn-around time effects—allowing ions with opposite velocities to obtain a distribution in their initial potential energies (spatial spread). The potential energy surface of the TI source is shown in Fig. 5. Filament and first lens are floated at 10 V. Ions formed on a hot metal at a temperature of 1800 K [18], corresponding to a thermal energy of 230 meV are accelerated to 35 eV by the second and third lenses. The ion beam enters a 10 cm cylindrical tube kept at zero potential (ground), interfacing the ion source optics and orthogonal region. The long cylinder facilitated the formation of a beam with small angular divergence by projecting the focal point at longer distances. A set of side deflectors was installed at the entrance of the cylinder to shape the beam and maintain transmission. Weak positive potentials (∼1 V) were found to have a significant effect on the spatial and energy distributions of the ions entering the orthogonal gate.

In a phase space diagram, the turn-around time effect is defined by ions corresponding to pairs of points symmetrical about the horizontal axis having a common starting position and opposite velocities. For uncorrelated distributions of ions, the minimum arrival time spread can be approximated by such an ion pair with the maximum velocity spread. For ions desorbing from surfaces, the case encountered in the delayed extraction technique, the phase space along the mass analysis axis is linear with velocities in the forward direction. In oTOF MS, ions can be forced into non-linear phase space distributions with velocities extending in both directions.

Fig. 6 is an example of the phase space distribution for the ^{142}Nd ions at the centre of the orthogonal gate. For −36 V on the lens the distribution forms a sigmoidal shape, represented by the open circles (60 ions). Points with the maximum velocities have obtained a spatial separation and they fly with different velocities

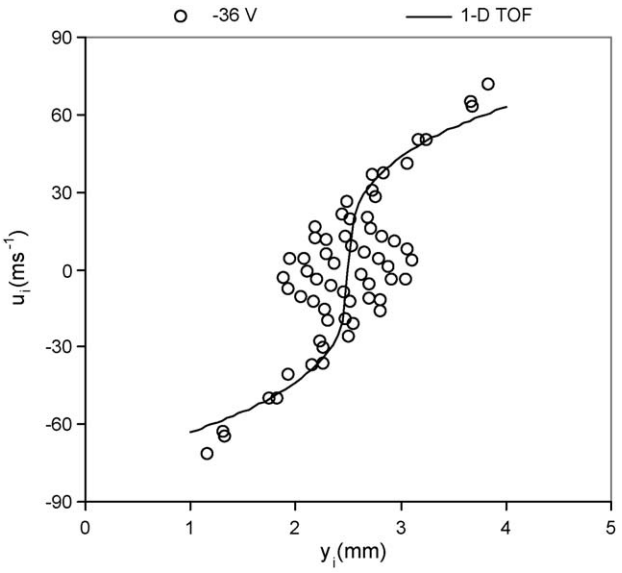

Fig. 6. Phase space distribution of ions for the TI source in the TOF direction. Individual points represent ions transmitted into the gate. A sigmoidal distribution is obtained for −35 V on the middle lens. The solid curve is used to approximate the distribution and perform one-dimensional TOF calculations.

towards the detector. The distribution has not clearly resolved into its spatial and velocity components and turn-around time effects are present only for the ions at the centre of the beam. With reference to Fig. 6, the turn-around time for ^{142}Nd ions with the maximum velocity of 30 ms^{-1} and the same starting positions is 3.9 ns, close to the value of ∼4 ns (FWHM) observed experimentally. Conversely, a direct calculation using the turn-around time formula [7] for a time spread of ∼4 ns would predict a maximum velocity spread of 30 ms^{-1} which is an underestimation of the effective velocity spread assuming a correlated distribution as described above. Ions with greater velocities have obtained a spatial separation before extraction and the differences in their flight times are corrected by adjusting the voltage ratio. The effective spatial spread is 3.0 mm with an energy spread of 4 meV, independent of *m*/*z*. For a 3 mm spatial spread space focusing theory predicts an extraction pulse of 800 V ($\xi = 0.28$) and in practice defines the lowest voltage ratio that can be used for time-focusing ions in the 67 cm long configuration and a total energy of 3.5 keV.

A sigmoidal distribution was also produced for the EI source with turn-around time effects present for the ions at the centre of beam. The estimated initial spatial spread was 3.0 mm with an energy spread of 11 meV, independent of *m*/*z*. The phase space diagram was approximated with a correlated function, similar to that shown in Fig. 6 for ^{142}Nd ions. The mirrored arrival time distributions obtained by one-dimensional calculations for the ^{129}Xe ions are shown in Fig. 7 as a function of initial ion velocity (a) and starting position (b). The distributions are folded twice and ions with opposite velocities and a spatial separation exhibit identical flight times with ions at the centre of the beam. The maximum and minimum arrival times correspond to ions with opposite velocities accelerating over the same distance within the first field.

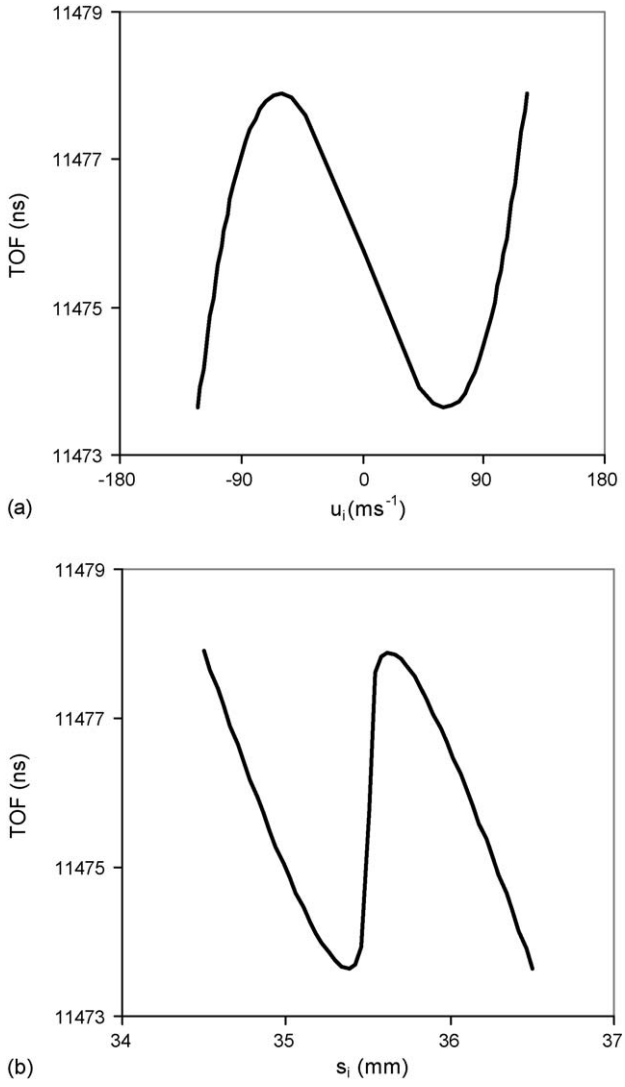

Fig. 7. Calculated arrival time distributions as a function of initial velocity (a) and acceleration distance (b) for ^{129}Xe.

Calculated focusing curves for the ^{142}Nd and ^{129}Xe ions using the correlated functions to approximate SIMION phase space distributions are compared with experimental results, as illustrated in Fig. 2. The calculated optimum voltage ratio for ^{142}Nd is shifted by $\delta\xi = 0.02$ which corresponds to an error of 40 V across the first field. For the same distance, the ratio for ^{129}Xe falls on the optimum value determined experimentally. A reduction in the time spread of the ions is observed as the focal point is projected closer to the orthogonal acceleration region. The optimum ratio required to focus ions deviates for the 45 cm configuration, with an error of 20 V. The effect is partly attributed to a change in the flight angle of the ions and the acceptance angle of the instrument. In our experiments, the flight angle becomes steeper as the energy of the ions in the TOF direction is increased by applying higher extraction pulses. The acceptance angle of the instrument reduces as the detector, centred in the flight tube axis, is displaced to the shorter distances. Although the offset of the theoretical focusing curves on the time spread axis in Fig. 2 cannot be easily interpreted, one-dimensional calculations of

the ion's flight times using non-linear space-velocity correlated functions show similar trends to those observed experimentally and can provide useful information on the behaviour of virtual sources.

4. Theory

Experimental results and numerical analysis demonstrating the formation of correlated phase space distributions of ions motivated us to seek for an analytical solution to the time-focusing properties in oTOF MS. Assuming a linear space-velocity correlated distribution in the TOF direction, first and second-order focusing conditions are derived using a composite Taylor expansion of the flight time equation to describe ions moving in opposite directions. The analysis considers a point source with an isotropic kinetic energy distribution independent of the ion's mass. Ions undergo prompt acceleration and are directed through the optics into a field-free region. A lens system is incorporated to correct for the initial angular divergence of the beam and can be arranged to produce a focal point near/at the source exit slit. The cross-section of the beam at any distance thereafter, is a function of the angular divergence at the source focal point and the total energy of the ions. Provided that enough time is allowed for the slowest ion to fill the orthogonal gate, all masses will acquire a common spatial and energy spread at the onset of the extraction pulse. A schematic diagram of the oTOF geometry is shown in Fig. 8(a). The extremes of the beam are defined by ions with the greater velocities. Fig. 8(b) shows the ideal case of a linear distribution.

The ion ensemble is divided into two groups to describe ions with opposite initial velocities. The flight time is calculated using two ions with mean position-velocities corresponding to each of the two distributions, as shown in Fig. 8(b):

$$t = \begin{cases} t_i, & (s_i, u_i \geq 0) \\ t_j, & (s_j, u_j < 0) \end{cases} \tag{1}$$

where i and j represent ions in the forward and backward distributions, respectively. Eq. (1) is a continuous function of the initial ion velocity since $\lim_{u_i \to 0} t_i = \lim_{u_j \to 0} t_j = t(s_0, 0)$ where $t(s_0, 0)$ is the flight time of the reference ion with zero initial velocity that is accelerated over a distance s_0 within the first field of length s. Ions in the forward distribution undergo an accelerating motion following the onset of the extraction pulse. In a two-stage acceleration system, the ith ion with the average velocity u_i accelerates over a distance s_i with an overall flight time:

$$t_i = \frac{u_{si} - u_i}{a_s} + \frac{u_{di} - u_{si}}{a_d} + \frac{D}{u_{di}} \tag{2}$$

where a_s and a_d are the constant accelerations in the first and second electric fields of lengths s and d, respectively. The position of the detector is defined by the length of the field-free region D, and u_{si}, u_{di} are the velocities at the end of each electric field:

$$u_{si} = \sqrt{u_i^2 + 2s_i a_s} \tag{3}$$

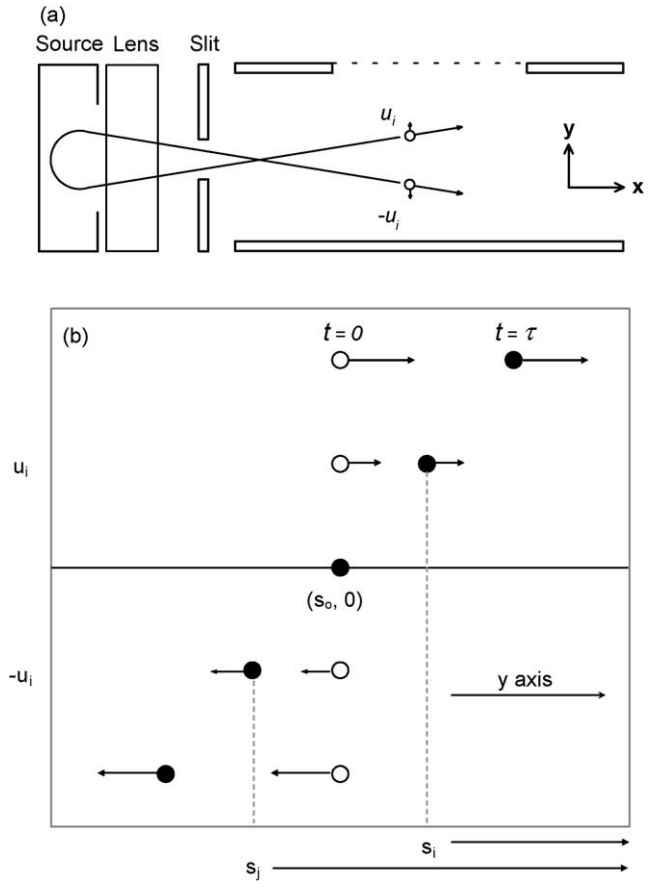

Fig. 8. A schematic of an oTOF MS showing source ion optics and the formation of a correlated beam entering the orthogonal gate (a). Starting "◯" and final "●" distributions of ions in the TOF direction from the point source to the orthogonal gate (b).

$$u_{di} = \sqrt{u_i^2 + 2s_i a_s + 2da_d} \tag{4}$$

The second distribution encompasses ions with initial velocities in the opposite direction. The jth ion with the average velocity ($u_j = -u_i$) decelerates and returns to its original position. The subsequent motion in the first field is that of an ion with a starting velocity u_i accelerating over a distance s_j, $s_j > s_i$. It is this difference in the acceleration distances of the two ions considered that allows for focusing to occur. The overall flight time is determined by the velocities at the end of each electric field:

$$t_j = \frac{u_{sj} + u_i}{a_s} + \frac{u_{dj} - u_{sj}}{a_d} + \frac{D}{u_{dj}} \tag{5}$$

$$u_{sj} = \sqrt{u_i^2 + 2s_j a_s} \tag{6}$$

$$u_{dj} = \sqrt{u_i^2 + 2s_j a_s + 2da_d} \tag{7}$$

The forward and backward distributions are symmetric relative to s_0. By assuming a point source at the s_0 starting position, ions form a linear distribution in phase space (y plane) during a virtual time delay. The virtual time delay represents the mass dependent arrival time from the source to the effective region of the orthogonal gate. The starting and final distributions of

the ions from the source to the orthogonal gate are shown in Fig. 8(b).

The acceleration distance is defined by the starting position, initial velocity and virtual time delay τ:

$$s_i = s_0 - u_i\tau \tag{8}$$

$$s_j = s_0 + u_i\tau \tag{9}$$

Eqs. (8) and (9) are substituted into (2) and (5), respectively, and then expanded in a Taylor series in either initial position or initial velocity. In this case, the flight time of the reference ion is approximated in terms of the ion with the average velocity in the forward distribution. Neglecting third and higher order terms:

$$t_0 = t_i - u_i\frac{\partial t_i}{\partial u_i} + \frac{u_i^2}{2}\frac{\partial^2 t_i}{\partial u_i^2} \tag{10}$$

where $\delta t_i = t_0 - t_i$ is the time spread for the forward distribution. Taylor expansion for the backward distribution:

$$t_0 = t_j + u_i\frac{\partial t_j}{\partial u_i} - \frac{u_i^2}{2}\frac{\partial^2 t_j}{\partial u_i^2} \tag{11}$$

is an estimation of the error in the arrival time spread of the reference ion relative to the ion with the average negative velocity, $\delta t_j = t_0 - t_j$. The overall arrival time spread is the sum of the errors from each distribution, $\delta t = \delta t_i + \delta t_j$:

$$\delta t = u_i\left(\frac{\partial t_j}{\partial u_i} - \frac{\partial t_i}{\partial u_i}\right) + \frac{u_i^2}{2}\left(\frac{\partial^2 t_i}{\partial u_i^2} + \frac{\partial^2 t_j}{\partial u_i^2}\right) \tag{12}$$

First-order focusing requires that the first term in the truncated series is zero:

$$\frac{\partial t_j}{\partial u_i} - \frac{\partial t_i}{\partial u_i} = 0 \tag{13}$$

The optimum distance for the detector where the arrival time spread is minimized can be expressed as:

$$D = \frac{\begin{array}{c}(a_d/a_s)(2 + (u_{ci}/u_{si}) + (u_{cj}/u_{sj})) + (u_{ci}/u_{di}) \\ + (u_{cj}/u_{dj}) - (u_{ci}/u_{si}) - (u_{cj}/u_{sj})\end{array}}{(a_d u_{ci}/u_{di}^3) + (a_d u_{cj}/u_{dj}^3)} \tag{14}$$

where $u_{ci} = \tau a_s - u_i$ and $u_{cj} = \tau a_s + u_i$ are the correlated velocities for the ith and jth ions, respectively. The velocity ratios are defined according to the following dimensionless mass independent relationships:

$$l_i = \frac{u_{ci}}{u_{si}} = \frac{(h/2)\sqrt{\lambda/s\kappa_s} - \sqrt{d\kappa_d}}{\sqrt{s_i\lambda + d\kappa_d}} \tag{15}$$

$$l_j = \frac{u_{cj}}{u_{sj}} = \frac{(h/2)\sqrt{\lambda/s\kappa_s} + \sqrt{d\kappa_d}}{\sqrt{s_j\lambda + d\kappa_d}} \tag{16}$$

$$m_i = \frac{u_{ci}}{u_{di}} = \frac{(h/2)\sqrt{\lambda/s\kappa_s} - \sqrt{d\kappa_d}}{\sqrt{s_i\lambda + d(1+\kappa_d)}} \tag{17}$$

$$m_j = \frac{u_{cj}}{u_{dj}} = \frac{(h/2)\sqrt{\lambda/s\kappa_s} + \sqrt{d\kappa_d}}{\sqrt{s_j\lambda + d(1+\kappa_d)}} \tag{18}$$

and the effective flight paths for the two ions:

$$n_i = \frac{a_d u_{ci}}{u_{di}^3} = \frac{(h/2)\sqrt{\lambda/s\kappa_s} - \sqrt{d\kappa_d}}{2[s_i\lambda + d(1+\kappa_d)]^{3/2}} \tag{19}$$

$$n_j = \frac{a_d u_{cj}}{u_{dj}^3} = \frac{(h/2)\sqrt{\lambda/s\kappa_s} + \sqrt{d\kappa_d}}{2[s_j\lambda + d(1+\kappa_d)]^{3/2}} \tag{20}$$

where λ is the ratio of the electric fields, $\lambda = a_s/a_d = \varepsilon_s/\varepsilon_d$, κ_s and κ_d are the ratios of the average initial ion kinetic energy to the total energies stored in the two fields, respectively, $\kappa_s = T_i/U_s$ and $\kappa_d = T_i/U_d$ and $h = s_0 - s_i = s_j - s_0$. The first-order focusing constraint can then be reduced as:

$$D = \frac{(1/\lambda)(2 + l_i + l_j) + m_i + m_j - l_i - l_j}{n_i + n_j} \tag{21}$$

Eq. (21) is the mass independent focal distance for the ions in oTOF MS when a linear space-velocity correlated distribution is considered. The requirement for second-order focusing is determined by the second term in the composite Taylor series:

$$\frac{\partial^2 t_i}{\partial u_i^2} + \frac{\partial^2 t_j}{\partial u_i^2} = 0 \tag{22}$$

and the additional focusing condition to be simultaneously satisfied is expressed as:

$$D = \frac{\begin{array}{c}((1-\lambda)/\lambda)[pl_i(1-l_i^2) + l_j(1-l_j^2)] \\ + pm_i(1-m_i^2) + m_j(1-m_j^2)\end{array}}{pn_i(1-3m_i^2) + n_j(1-3m_j^2)} \tag{23}$$

where p is the ratio of the correlated initial ion velocities:

$$p = \frac{u_{cj}}{u_{ci}} = \frac{h + 2s\kappa_s}{h - 2s\kappa_s} \tag{24}$$

Analytical solutions for first and second-order focusing conditions for the ideal case of linear distributions show that the spatial and velocity aberrations to the arrival time spread of the ions are removed and perfect time focusing is achieved. Linear distributions in phase space can be used to approximated ion sources and/or beams with small phase space volumes. Alternatively, a narrow slit can be used to transmit ions only from the centre of a beam with large angular divergence.

5. Conclusions

The concept of space-velocity correlated distributions in oTOF MS has been explored experimentally and theoretically. It is demonstrated that variations in the time focusing properties of the system are directly related to the initial spatial and velocity distributions of the ions in the orthogonal gate. Ion optics can be used to resolve spatial and velocity components of the ion beam. The formation of non-linear phase space distributions is a more realistic situation, compared with the ideal case of a linear distribution, and can be used for reducing the contribution of the turn-around time to the final resolving power of the instrument. Controlling the angular divergence of the beam is

essential for enhancing resolving power in oTOF MS. Optimum virtual sources for reflectrons are specific to the instrument and the source employed for ion production. Detector displacements can identify such focal distances in the field-free region of the spectrometer, which can then be used to study the effect of a reflectron.

References

[1] G.J. O'Halloran, R.A. Fluegge, J.F. Betts, W.J. Everett, Technical Report No. ASD-TDR-62-644, The Bendix Corporation, Research Laboratory Division, 1964, Parts I and II.
[2] J.H.J. Dawson, M. Guilhaus, Rapid Commun. Mass Spectrom. 3 (1989) 155.
[3] A.F. Dodonov, I.V. Chernushevich, V.V. Laiko, Proceedings of the 12th International Mass Spectrometry Conference, Amsterdam, The Netherlands, 1991, p. 153.
[4] I.V. Chernushevich, A.V. Loboda, B.A. Thomson, J. Mass Spectrom. 36 (2001) 849.
[5] A.V. Loboda, S. Ackloo, I.V. Chernushevich, Rapid Commun. Mass Spectrom. 17 (2003) 2508.
[6] M. Lewin, M. Guilhaus, J. Wildgoose, J.B. Hoyes, R.H. Bateman, Rapid Commun. Mass Spectrom. 16 (2002) 609.
[7] W.C. Wiley, I.H. McLaren, Rev. Sci. Instrum. 26 (1955) 1150.
[8] S.M. Colby, J.P. Reilly, Anal. Chem. 68 (1996) 1419.
[9] M. Vestal, P. Juhasz, J. Am. Soc. Mass Spectrom. 9 (1998) 892.
[10] M. Guilhaus, D. Selby, V. Mlynski, Mass Spectrom. Rev. 19 (2000) 65.
[11] P.V. Bondarenko, R.D. MacFarlane, Int. J. Mass Spectrom. Ion Process. 160 (1997) 241.
[12] R.J. Cotter, Time-of-Flight Mass Spectrometry, American Chemical Society, Washington, DC, 1997.
[13] R. Antoine, L. Arnaud, M. Abd El Rahim, D. Rayane, M. Broyer, Ph. Dugourd, Int. J. Mass Spectrom. 239 (2004) 1.
[14] R. Stein, Int. J. Mass Spectrom. Ion Process. 132 (1994) 29.
[15] Y.H. Chen, M. Gonin, K. Fuhrer, A.F. Dodonov, C.S. Su, H. Wollnik, Int. J. Mass Spectrom. 185/186/187 (1999) 221.
[16] A.F. Dodonov, V.I. Kozlovski, I.V. Soulimenkov, V.V. Raznikov, A.V. Loboda, Z. Zhen, T. Horwath, H. Wollnik, Eur. J. Mass Spectrom. 6 (2000) 481.
[17] V.V. Laiko, A.F. Dodonov, Rapid Commun. Mass Spectrom. 8 (1994) 720.
[18] D. Papanastasiou, PhD Thesis, MMU, Manchester, UK, 2005.
[19] D.A. Dahl, SIMION 3D, v7.0, INEEL, 2000.